

Article

# Electrification of Oil and Gas Platforms by Wind Energy

Nejm Saadallah <sup>\*,†</sup>  and Yngve Heggelund <sup>†</sup> 

NORCE Norwegian Research Centre, P.O. Box 22, Nygårdstangen, NO-5838 Bergen, Norway

\* Correspondence: nsaa@norceresearch.no

† These authors contributed equally to this work.

**Abstract:** In this paper, we address the problem of high greenhouse gas emissions from oil and gas platforms in Norway. We look at the potential of integrating an energy system composed of wind turbines and battery systems to unload the electrical power generated by gas turbines being the main source of emissions today. We propose a simulation model of the energy system, the power demand, the available wind speed, and different control strategies. By putting the models together, we evaluate the performance of various compositions of the system and determine their impact on emissions and battery lifetime. The numerical results show that changing today's practices has great potential to reduce greenhouse gases, with amounts varying between 30% and 80% compared with today's level.

**Keywords:** wind energy; energy system integration; energy system simulation; greenhouse gas emissions; stochastic simulations; energy storage; offshore technology

## 1. Introduction

Currently, approximately 25% (12.1M tonnes of 48.9M tonnes as of 2021) [1] of Norway's CO<sub>2</sub> emissions comes from oil and gas installations in the North Sea. These emissions are mainly due to the usage of gas turbines, which provide electrical power to the processes needed for oil and gas production. These emissions need to be significantly reduced in order to meet the goals of the European green deal of reducing the net greenhouse gas emissions by at least 55% by 2030 compared to 1990 levels [2].

To reduce the usage of gas turbines, one possibility is to supply electrical power from land. This can, however, be challenging and costly for many facilities, especially those furthest from the shore and in deep waters. In [3], the authors highlight the challenges due to the large investments and high economical risks in relation to electrification of offshore installations close to Saudi Arabia and discuss the trade-offs between using HVAC and HVDC cables. In the North Sea, there are additional challenges regarding the bottom depth and topography, and it may be more cost-efficient to install wind turbines close to production facilities. The North Sea has very good wind conditions [4], and exploiting these resources provides an opportunity to transition to renewable energy production for future energy needs while at the same time reducing the climate impact of the ongoing production of oil and gas.

A main challenge with wind energy is the variability of the wind resources. The power demands of the production facilities are also variable and unpredictable to some degree. This provides a challenge for the decarbonization of electricity production since gas turbines will have to be left running in idle mode to rapidly take over electricity production when wind power is not sufficient. This imbalance between available power and demand can be alleviated by adding energy buffers. If the energy buffer capacity is sufficient to last during the startup phase of the gas turbines, it will be possible to completely shut off the gas turbines over long periods and only start them when needed. This way of operating the gas turbines will significantly reduce the overall climate gas emissions since significant amounts of CO<sub>2</sub> are emitted even when the turbines are running idle. However,



**Citation:** Saadallah, N.; Heggelund, Y. Electrification of Oil and Gas Platforms by Wind Energy. *Energies* **2023**, *16*, 3062. <https://doi.org/10.3390/en16073062>

Academic Editor: Adrian Ilinca

Received: 22 February 2023

Revised: 24 March 2023

Accepted: 26 March 2023

Published: 27 March 2023



**Copyright:** © 2023 by the authors. Licensee MDPI, Basel, Switzerland. This article is an open access article distributed under the terms and conditions of the Creative Commons Attribution (CC BY) license (<https://creativecommons.org/licenses/by/4.0/>).

the capacities of the buffers are subject to space and weight constraints at or close to the wind turbines and the production facilities.

Our approach is to place battery storage in the wind turbines' foundations. In our study, we assume a floating foundation of a semi-submersible type, where battery systems can be placed. We model the energy system in a dynamical model, which includes electricity generation from the wind, battery storage, and gas turbines. The boundary conditions are time series of wind speed and electricity demand on the production facility. The energy system builds on a model that was implemented in the Modelica language published previously [5]. In [6], the authors suggest an alternative based on LabView for micro-grid modelling. Another alternative that relies on Modelica can be found in [7]. However, none of the mentioned alternatives address the uncertainty in wind speed and load. In [8], the authors suggest a model that is based on a general algebraic modelling system (GAMS) and which does account for uncertainty in the wind speed and demand. The authors in [8] formulate the problem as a frequency dynamic control problem, which imposes important assumptions on the system's inertia and on the system's components. In the current study, we regard the demand as uncertain and not controllable. Our approach addresses uncertainties by simulating ensembles of realizations of wind speed and demand time series. As for our technical choices, we have adopted Python for practical software integration reasons that are outside the scope of this paper.

Our model is used to simulate the behaviour of this closed energy system under different conditions, such as variable wind speed, power demand, numbers of wind turbines, and energy storage capacity. A main question is how the system can be controlled to minimize the usage of gas turbines (and thereby minimize CO<sub>2</sub> emissions) while maintaining a stable system with minimal power imbalance.

Section 2 gives a description of the modelling approach, including a description of the boundary conditions (wind and power demand). Section 3 presents the battery degradation estimation model. Section 4 gives an overview of the control approach. Section 5 presents the simulation results. Finally, Section 6 concludes the paper.

## 2. Computational Models

In this section, we explain the various sub-models and the equations describing their dynamics.

### 2.1. Principles

This study considers a simulation model of a power system. The principle behind the system was to combine wind turbines, gas turbines, and a battery system to address variable power demands. In that respect, the use cases were defined by samples of power demand, available wind resources, and the power capacity for the energy components (wind turbines, batteries, and gas turbines). An important aim of this paper was to find a control strategy that minimizes the usage of gas turbines while keeping the local power grid in balance. The architecture of the simulation model is illustrated in Figure 1. The simulation model took as external inputs time series samples of wind speed and power demand and simulated the system dynamics according to a control strategy. We assumed that the control can obtain access to current load (power demand), current state of charge of the battery, and current available power at both the wind turbines and gas turbines. The control loop time here is given by the discrete time interval  $\Delta t$ , which we will refer to as the decision time interval. The sampling models will be further explained in Sections 2.6 and 2.7. The scope of the control strategy shown in the figure was mainly to decide on the power set points for the gas turbines, wind turbines, and batteries. The possible imbalance between the power supply and demand was captured by the energy balance principle in the variable  $P_{imb}$ . In practice, small energy imbalances are handled using power stabilizing units. Furthermore, the power imbalance combined with the amount of emission gases  $E_{CO_2}$  (and  $E_{NO_x}$ ) were used to assess both the stability and quality of the system. Informally, we considered the system to

be stable when it was well balanced and to be of high quality when it was both balanced and had low greenhouse gas emissions. This will be further explained in Section 2.8.

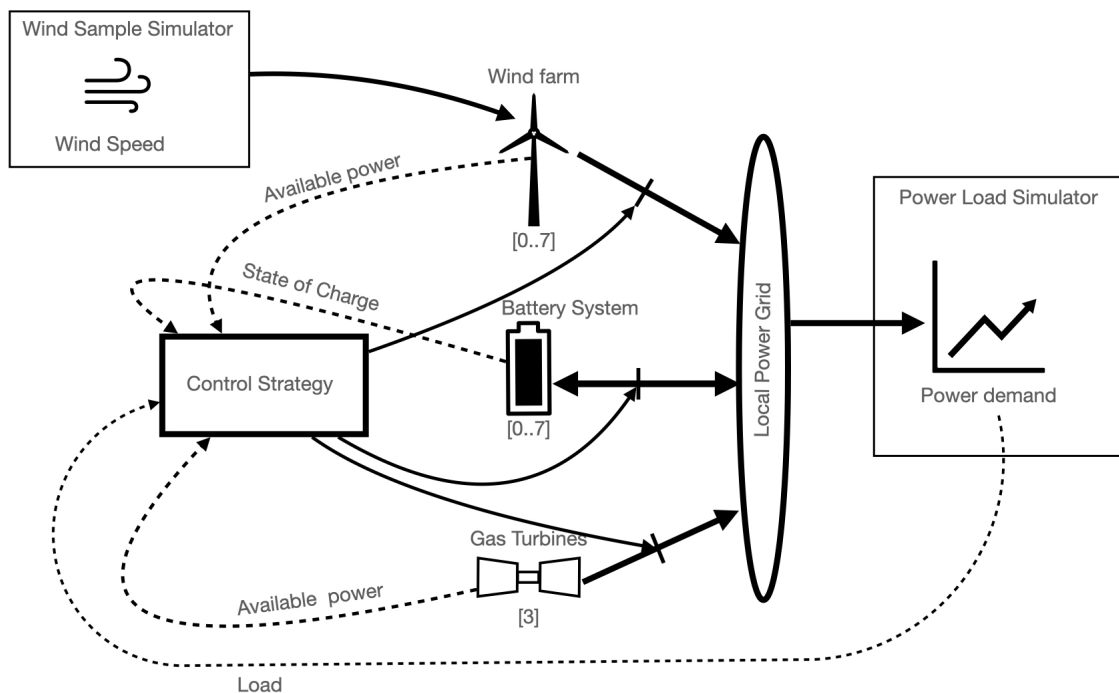


**Figure 1.** Overview of the micro-grid simulation model.

The model was used to perform stochastic simulations with 50 wind speed and power demand samples lasting for a period of 7 days. Using those samples, we simulated multiple design scenarios by varying the number of wind turbines and battery capacities. For practical reasons, we targeted a fast-running simulation model and have deliberately chosen to model the system using simplified energy components in the power domain rather than complex energy components in the electrical domain.

## 2.2. System Balance

The local grid component in Figure 1 models the balance between the power supply and power demand. Note that the grid model is a so-called *off-grid* power system, meaning that there was no main grid that could act as a regulation reserve to keep the whole system in power balance, as is the case in [9]. Equation (1) describes the power balance between the involved components, stating that the balance sheet  $P_{imb}$  is the sum of the wind power  $P_{wind}$  (always positive), the gas turbine power  $P_{gt}$  (always positive), the battery power  $P_{bat}$  (positive or negative), and the power demand  $P_d$  (always negative). Intuitively, a well-balanced grid is one that keeps  $P_{imb}$  as close as possible to zero, thus reducing the need for power stabilization units.

$$\left\{ \begin{array}{l} P_{wind} + P_{gt} + P_{bat} + P_d = P_{imb} \\ P_{wind}, P_{gt} \in \mathbb{R}_{\leq 0} \\ P_d \in \mathbb{R}_{\leq 0} \\ P_{bat}, P_{imb} \in \mathbb{R} \end{array} \right. \quad (1)$$

## 2.3. Gas Turbine Model

The dynamic of gas turbine generators can be modelled as a combined cycle power plant [10], but that would require significant details about the generator components. In the context of this paper, an important aspect of the gas turbines' dynamic is that they take a

significant time before they become fully operational. To capture that aspect, we modelled the available power of a gas turbine as a function of its state and determined the maximum ramp-up and ramp-down speeds at any given time from the power generated at that particular time. We also assumed that the combustion fuel was unlimited and that gas turbines can be controlled with power set-points that can be chosen by the operator or some control unit. The generated power  $P_i$  of a gas turbine  $i$  relates the power set point  $SP_i$  through Equation (2) using pre-subscribed (measurable) maximum ramp-up and ramp-down speeds  $v_u, v_d$ , respectively, as functions of the gas turbine generating power (state), as shown in Figure 2 (left). Likewise,  $E_{i,CO_2}$  and  $E_{i,NO_x}$  are both functions of the generated power from Figure 2 (center and right). Note that during the ramp-up phase, the emissions are larger than zero even when the turbines are producing no or close to no power.

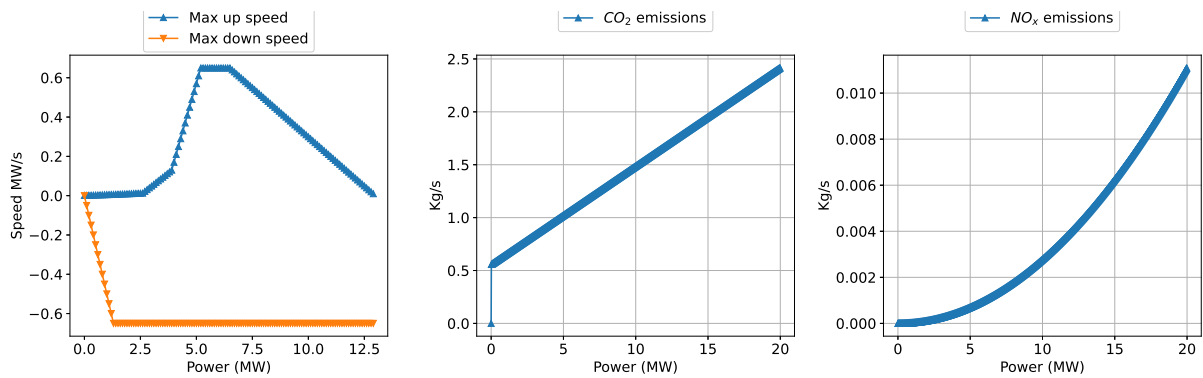


**Figure 2.** Maximum ramp-up and ramp-down, CO<sub>2</sub>, and NO<sub>x</sub> emissions, all as functions of the gas turbine-generated power.

Figure 3 shows the fastest possible ramp-up from zero to maximal power output and back to zero.

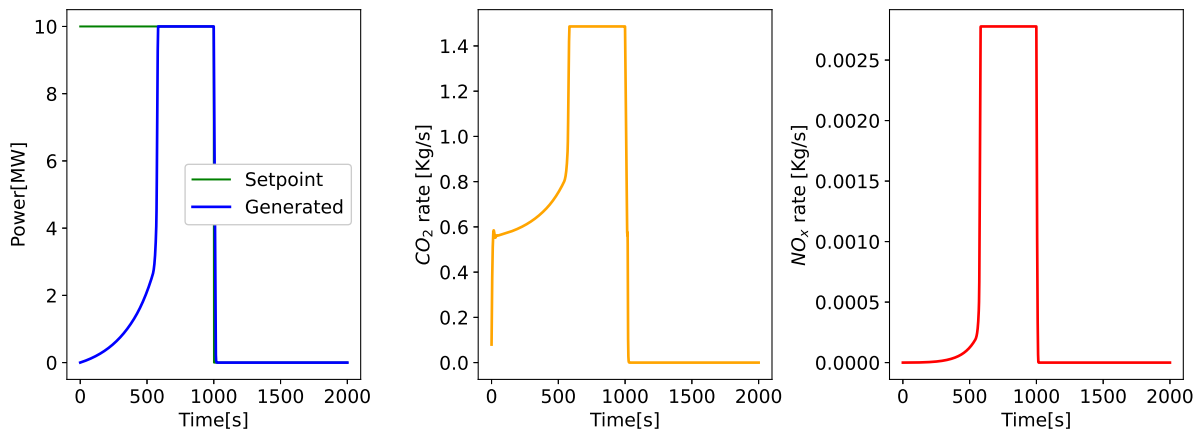


**Figure 3.** Fastest possible ramp-up of a gas turbine from zero to maximal power output and back to zero and its corresponding greenhouse gas emission rate.

$$\begin{cases} \Delta P_i = \min(v_u \cdot \Delta t, SP_i - P_i), & \text{if } SP_i > P_i \\ \Delta P_i = \max(v_d \cdot \Delta t, P_i - SP_i), & \text{if } SP_i < P_i \\ \Delta P_i = 0, & \text{if } SP_i = P_i \end{cases} \quad (2)$$

We assumed that the total generated power from the three gas turbines  $P_{gt}$  and the total emissions were the sum of the power generated and gas emissions at each gas turbine, respectively; see Equation (3).

$$\begin{cases} P_{gt} = \sum_{i=1}^{i=3} P_i, & E_{CO_2} = \sum_{i=1}^{i=3} E_{i,CO_2}, & E_{NO_x} = \sum_{i=1}^{i=3} E_{i,NO_x} \end{cases} \quad (3)$$

To control the gas turbines, we assumed a system that took one set point  $SP_{gt}$  and distributed that set point to three gas turbines by priority according to Equation (4). The point here was to not start a gas turbine unless it was necessary. For example, with  $SP_{gt} = 15$  MW, and  $\forall i, GTP_{i,max} = 12$  MW (maximum power generated by gas turbine  $i$ ), we obtained  $SP_1 = 12$  MW,  $SP_2 = 3$  MW, and  $SP_3 = 0$  MW.

$$SP_i = \min(SP_{gt} - \sum_{j=1}^{i-1} SP_j, GTP_{i,max}) \tag{4}$$

2.4. Wind Power Model

The wind power model relates wind speed,  $V$ , to available wind power,  $AWP$ , following Equation (5), where  $A$  is the swept area,  $\rho_{air}$  is the air density,  $N_{wt}$  is the number of wind turbines, and  $C_p$  is the performance power coefficient. In this paper, we used a 10 MW DTU reference wind turbine [11] with the characteristics shown in Figure 4. The rotor radius  $R$  was 89 m, and the density of air  $\rho_{air}$  was assumed to be constant at 1.225 kg/m<sup>3</sup>. The number of wind turbines,  $N_{wt}$ , were varied during the study. We neglected reduced power output due to wake and blockage effects in this study. The inclusion of these effects would require consideration of the wind farm layout and was deemed outside the scope of the current study.

We considered that wind power  $P_{wind}$  could be regulated with a power set point  $SP_{wt}$  to power levels below  $AWP$ , as is shown in Equation (5).

$$\left\{ \begin{array}{l} AWP = \frac{1}{2} \cdot \rho_{air} \cdot A \cdot C_p \cdot V^3 \cdot N_{wt} \\ A = \pi \cdot R^2, \\ P_{wind} = \min(AWP, SP_{wt}) \mid AWP \geq SP_{wt} \geq 0 \end{array} \right. \tag{5}$$

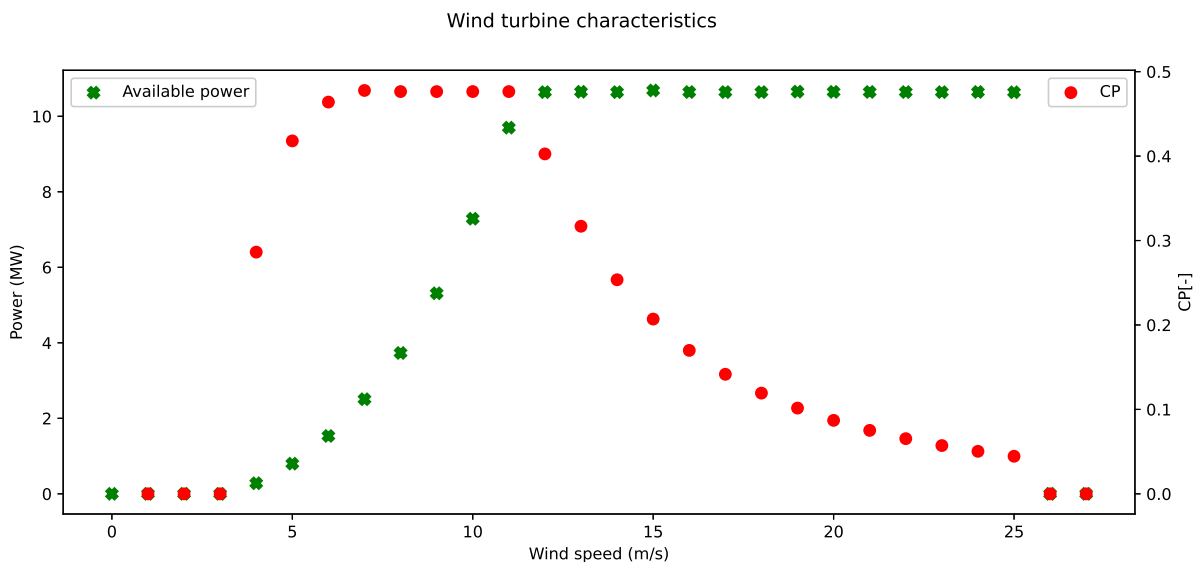


Figure 4. Characteristics of 10 MW DTU wind turbine.

2.5. Battery Model

The dynamic of the battery system is given by Equation (6). The charge rate,  $C_{rate}$ , is a number that tells how fast a battery can charge or discharge. A  $C_{rate}$  of 1 h<sup>-1</sup> means that the battery can fully charge from 0 to full capacity in 1 hour, and similarly for the discharge rate  $D_{rate}$ . Equation (6) states that the energy stored in the battery varies with the power  $P_{bat}$  and that  $P_{bat}$  is subject to limits  $C_{lim}$  and  $D_{lim}$ . These limits capture the notion that a filled battery cannot be filled more, as well as the fact that an empty battery cannot be drained. These limits, being functions of the state of charge of the battery ( $SoC$ ), were expressed

using two efficiency factors,  $\eta_d$  (discharging efficiency) and  $\eta_c$  (charging efficiency), both modelled as logistic functions that were parameterised with  $k_d, d_0$  and  $k_c, c_0$  respectively.

$$\left\{ \begin{array}{l} \frac{dE_b}{dt} = -P_{bat} \\ P_{bat} \in [C_{lim}, D_{lim}] \\ SoC = \frac{E_b}{E_{max}} \\ C_{lim} = -\eta_c \cdot C_{rate} \cdot E_{max} \\ D_{lim} = \eta_d \cdot D_{rate} \cdot E_{max} \\ \eta_d = \frac{1}{1 + e^{-d_0 \cdot (SoC - k_d)}} \\ \eta_c = 1 - \frac{1}{1 + e^{-c_0 \cdot (SoC - k_c)}} \end{array} \right. \quad (6)$$

To calibrate the parameters of the logistic functions  $\eta_c$  and  $\eta_d$ , we used data from [12]. The chosen battery was a lithium iron phosphate or LFP (lithium ferrophosphate) battery with a charge rate of  $C_{rate} = 0.5 \text{ h}^{-1}$  and a discharge rate of  $C_{rate} = 1 \text{ h}^{-1}$ . These types of batteries have characteristics that make them suitable for the current purposes, such as low cost, a high degree of safety, and long cycle life. After calibration, the logistic functions take the shape shown in Figure 5. The simulated state of charge (SoC) over some charge/discharge cycles fit very well with the measured data with a max absolute error of less than 5%; see Figure 6, which shows that modelling the charge/discharge efficiencies as logistic functions are good approximations.

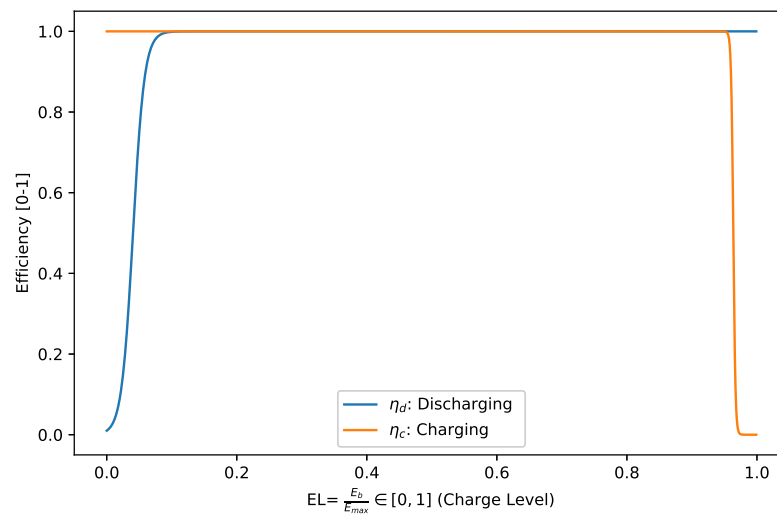


**Figure 5.** Efficiency factors  $\eta_c$  and  $\eta_d$  modelled using logistic functions with parameters  $\alpha = 0.04$  and  $\beta = 0.95$ .

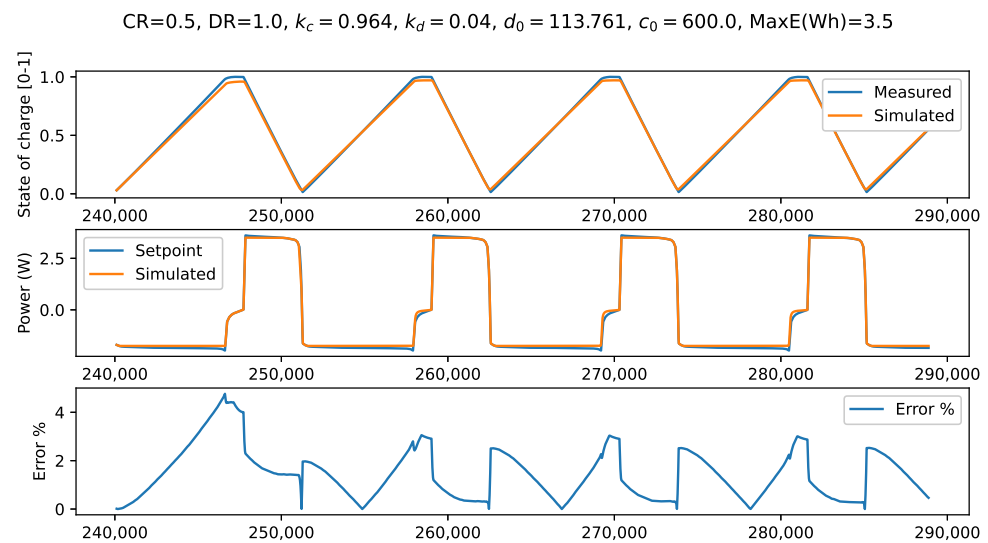


**Figure 6.** Battery model calibrated with sample data *SNL\_18650\_LFP\_25C\_0-100\_0.5-1C\_d\_timeseries.csv* from [12].

### 2.6. Demand Model

In principle, the power demand can be modelled in the time domain similarly to how we modelled the supply and storage. However, this required in-depth knowledge about the oil and gas platforms and their power demanding processes and was deemed to be outside the scope of our work. A more practical approach was to use a *measured* time series of the power produced by the gas turbines for a specific platform as the demand side of the power equation. This approach will, however, inherently be platform-specific.

A stochastically generated time series, which is based on and preserves some main features of the measured time series, provided flexibility to vary the demand side time series and alleviate the problems associated with relying on a single time series for the demand side modelling.

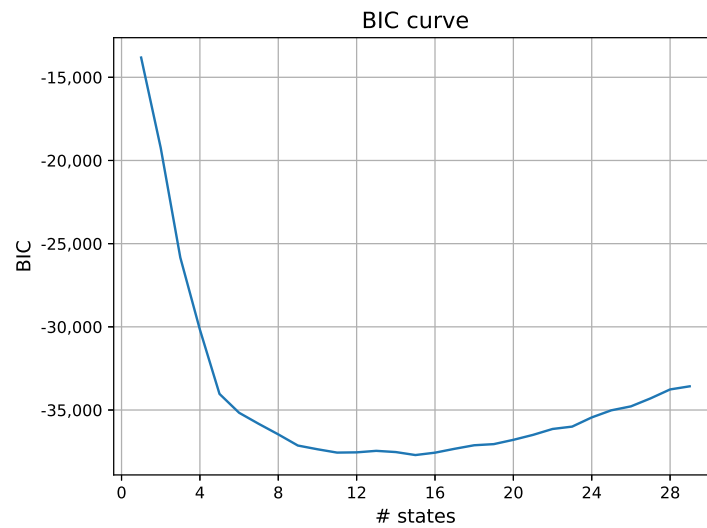
To generate a stochastic power demand time series that may be relevant for platforms of different sizes and different power characteristics, we decided to model the demand as a Gaussian hidden Markov model (GHMM) [13]. GHMM is a powerful technique for time series analysis and modeling and has been used in many application areas ranging from analysis of financial time series [14] to forecasting for water resource planning [15] and power system load forecasting [16]. A main assumption is that while the power demanding processes may vary between different platforms both in magnitude and frequency, some main features of the demand time series will remain similar between platforms since the processes themselves are similar. The GHMM approach enables us to vary parameters of the fitted model to characteristics and demand levels for platforms that are different from the one that the power demand time series originated from.

Some main processes for a typical oil and gas platform include drilling, injection, and the separation of liquids and gases, in addition to the base demand for the living quarters, but we generally have no way of correlating these processes to the measured time series. This means that both the state distributions and the transition probabilities between states need to be estimated.

The power demand cannot be considered to be normally distributed; clearly, the power demand will never be negative, and neither will any of the underlying processes demand negative power. A better approach is to assume a log-normal distribution, i.e., to fit the GHMM to the logarithm of the demand time series.

To fit a GHMM to the data, one must choose the number of states to fit. The expectation values and the standard deviations for each state in addition to the transition probabilities between states are then fitted to the data through likelihood maximization. The optimal number of states for the model is estimated using the Bayesian information criterion

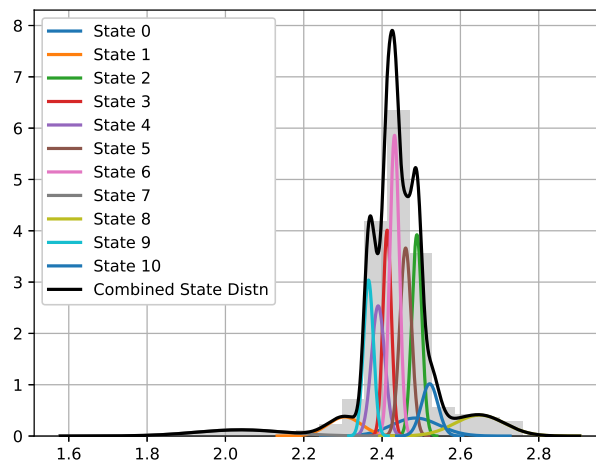
(BIC) [17], which is a trade-off between the number of parameters and the model fit. The BIC as a function of the number of states is shown in Figure 7.



**Figure 7.** BIC as a function of the number of states in the GHMM.

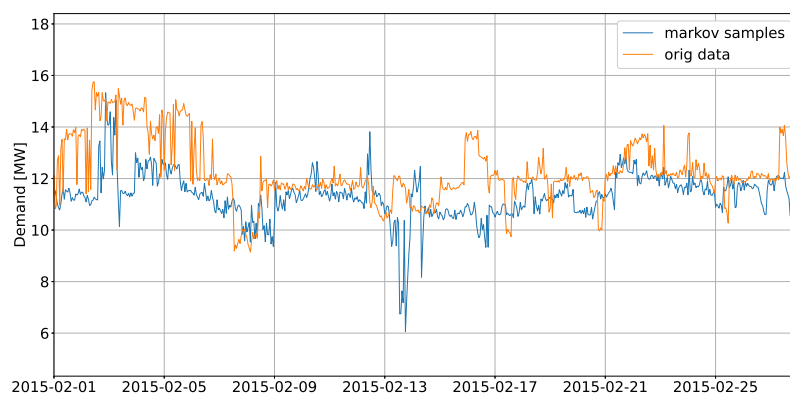
The BIC is lowest for 16 states. However, the difference in BIC between 11 and 16 states is negligible, so we have chosen to use 11 states in the model.

Figure 8 shows the distributions of the different states with their heights weighted by the stationary distribution for the transition probability matrix. The stationary distribution represents the fraction of time that the system is expected to be in the different states, given by the left eigenvector with eigenvalue 1 of the transition probability matrix. A joint probability distribution is also shown in the figure, together with a histogram of the values in the logarithm of the original time series (shown in gray bars), verifying that the model gives a probability distribution that is consistent with the measured data.



**Figure 8.** The histogram of the occurrence of each (log) demand level of the original time series (gray bars) together with the state distributions and the stationary joint probability distribution (solid black curve) for the GHMM.

An example of a random sampling from the fitted GHMM is shown in Figure 9. The sampled time series shares many features with the original data, e.g., the height and frequencies of the demand peaks and valleys and the same average demand level.



**Figure 9.** Sampling of the GHMM (blue) together with the original time series (orange).

### 2.7. Wind Speed Sampling

Time series of relevant wind speeds were downloaded from the ERA5 repository (<https://cds.climate.copernicus.eu>, accessed on 21 February 2023). The repository contains reanalysis data of past weather on an hourly time step and covers the earth on a 30 km grid up to a height of 80 km.

The downloaded data cover the years 2018 and 2019 at the closest grid point to 61.2N, 2.1E, which corresponds to the location of the Hywind Tampen offshore wind project, which will supply wind energy to the offshore oil and gas platforms at Snorre and Gullfaks off the west coast of Norway. The data were taken at a height of 100 m, which is approximately the hub height of the DTU 10 MW reference turbine (119 m).

A month of the time series of the wind speed data is shown in Figure 10.

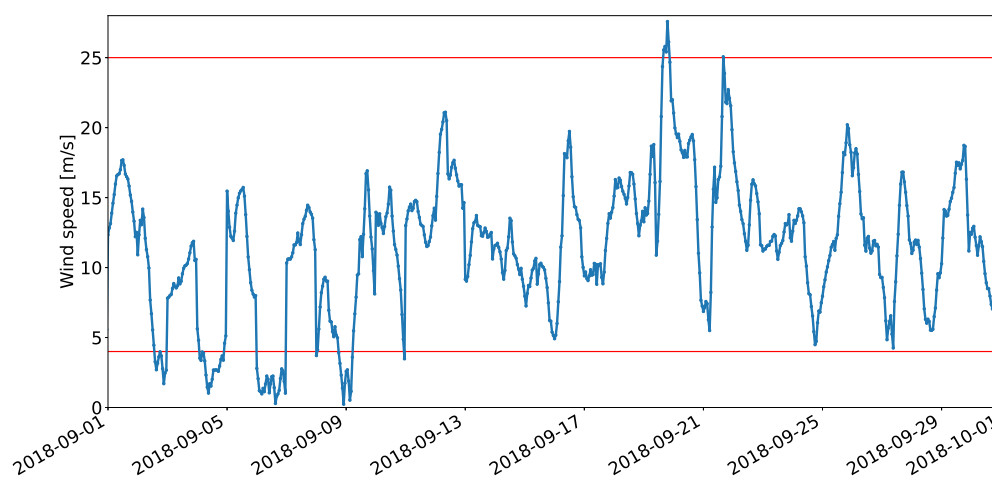


**Figure 10.** ERA5 wind speed at 100 m at Hywind Tampen in September 2018. The cut-in and cut-out wind speeds of the DTU 10MW turbine are marked with red lines.

### 2.8. Cost Model

We define two dependent cost functions that quantify the notions of system stability and quality modelled in Equation (7). The system stability is expressed using  $S_{st}$  as a function of the imbalance between the power generation and power demand  $P_{imb}$ . The function is defined in such a way that the system is considered to be stable ( $S_{st} \approx 1$ ) with small values for  $P_{imb} \approx 0$ , but the stability drops relatively quickly after a certain threshold in  $P_{imb}$ . We justify the tolerance for power imbalance by the fact that it can to some extent be compensated for using power stabilizing units. However, such units cannot compensate for large variations and should thus be reflected in poor system stability. The system quality  $S_{qt}$  is expressed using both the system stability and the amount of greenhouse gases emissions (limited to  $\text{CO}_2$ ). The normalized  $\text{CO}_2$  emission rate  $\hat{E}_{\text{CO}_2}$  is calculated using the emission rate  $E_{\text{CO}_2}$  divided by the maximum  $\text{CO}_2$  emission rate  $MAX_{\text{CO}_2}$ . In Figure 11,

we used  $MAX_{CO_2} = 4.5 \text{ kg s}^{-1}$ , corresponding to 3 gas turbines delivering 10 MW each. Figure 11 also shows that the system is defined to be high quality when it is stable and has low greenhouse gas emissions, and it is of poor quality otherwise.

$$\left\{ \begin{array}{l} S_{st} = \frac{1}{1 + 10^4 \cdot \hat{P}_{imb}} \\ \hat{P}_{imb} \in [-1, 1] \\ pu = 10 \text{ MW} \\ P_{imb} = \hat{P}_{imb} \cdot pu \\ S_{qt} = S_{st}^2 \times (1 - \sqrt{\hat{E}_{CO_2}}) \\ \hat{E}_{CO_2} = \frac{E_{CO_2}}{MAX_{CO_2}} \end{array} \right. \quad (7)$$

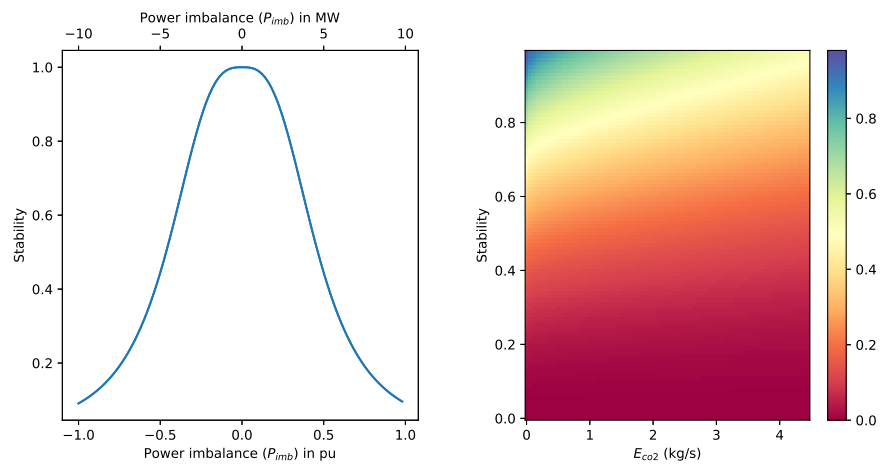


Figure 11. Plots of stability and quality from Equation (7).

### 3. Estimation of Battery Degradation

Typically, battery manufacturers consider a battery to have reached its end of life when it is at 80% of its initial capacity. The battery life is usually given by the number of cycles before its end of life. However, due to the intermittent usage pattern of batteries in this system with variable wind power and gas turbines that may either be switched on or off, estimating the number of battery charge-discharge cycles is not a trivial task. For this purpose, the rainflow counting algorithm developed by Matsuishi and Endo [18] can be used to identify the cycles and their ranges from time series data.

The relationship between cycle range and degradation can be estimated through empirical parameters. In Chawla et al. [19] and Alam et al. [20], the authors propose an exponential relationship between the state of charge (SoC) range,  $R$ , and the number of cycles the battery can experience at that range,  $C(R)$ , before the cycle-life is spent.

$$C(R) = AR^B \quad (8)$$

The LFP batteries used in this study have a quite long cycle-life of around 5000 cycles for 80% SoC swings. The corresponding cycle-life when the battery experiences lower SoC swings is usually not available from the manufacturers. However, based on the assumption that the batteries will provide more than twice the number of cycles when halving the SoC swings, Chawla et al. [19] proposes to set  $B = -1.483$ . The life curve for these parameters is shown in Figure 12. These estimates can be calibrated from recordings of actual usage patterns and the corresponding degradation of similar battery systems.

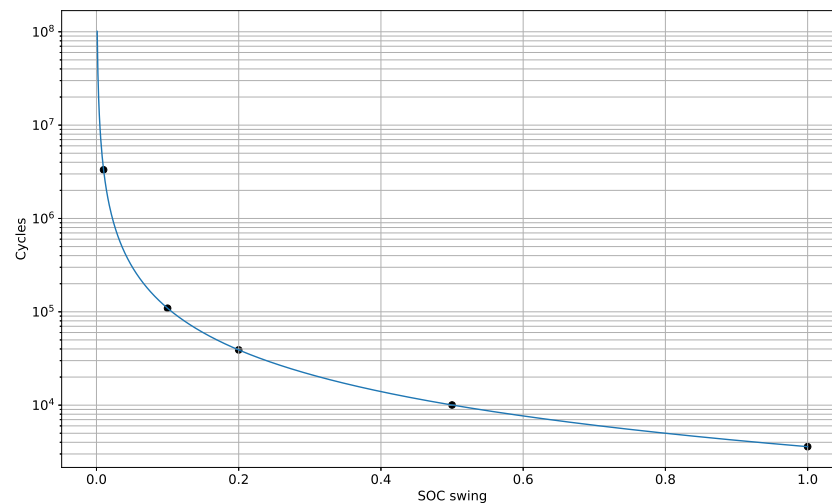


**Figure 12.** Proposed life curve for the LFP batteries. The dots are at 0.01, 0.1, 0.2, 0.5, and 1.0 SoC swings.

The rainflow counting algorithm counts either half or full cycles. Let  $S_j$  be defined such that

$$S_j = \begin{cases} \frac{1}{2} & \text{if } j \text{ is a half-cycle} \\ 1 & \text{if } j \text{ is a full-cycle} \end{cases} \quad (9)$$

and let  $\{(S_j, R_j); j = 1 \dots n\}$  be the cycles and their ranges identified by the rainflow counting algorithm.

The total degradation,  $D$ , can then be estimated based on all the identified half and full cycles and their ranges by using Equation (10).

$$D = \sum_{j=0}^n \frac{S_j}{AR_j^B} \quad (10)$$

Note: In this study, we only consider battery degradation due to usage. We do not consider degradation due to the environment, e.g., due to temperature variations or humidity. Such degradation will come in addition to the usage degradation above.

#### 4. Control Policies

The control of the energy system has multiple objectives. The main objective is to ensure a stable energy supply to meet the energy demand of the oil and gas platform, while the secondary objective is to minimize the CO<sub>2</sub> emissions. The third objective is to optimize the lifetime of the system components. It is, at the same time, an advantage if a control policy is explainable and easily implementable in practice.

Therefore, the general policy is always to give preference to using the available wind power. If the available wind power is not sufficient to meet the demand, power from the batteries will be used. If the state of charge of the batteries becomes low, the gas turbines are started according to the policy explained in Section 4.1. The gas turbines are stopped according to the policies explained in Section 4.2. Surplus energy will be used to charge the batteries. Surplus exceeding what the battery system is able to accept is curtailed. When the gas turbines are running, they will, after the start-up time, be able to provide sufficient power to meet the demand, plus additional power to charge the battery system, according to the policies explained in Section 4.3.

##### 4.1. Policy for When to Start the Gas Turbine System

When the state of charge of the battery system is low and decreasing, the gas turbines will have to be started to ensure a stable energy supply. As discussed in Section 2.3, the gas turbines takes some time to start producing power from the moment they are switched on.

The gas turbines, therefore, need to be given the signal to be switched on some time before the battery system is depleted.

The policy could be based on a preset state of charge limit of the battery system, which is shown in Figure 13. The policy in this case is simply to give the signal to switch on the gas turbines when the state of charge is less than the pre-computed low limit and to switch off the gas turbine when the state of charge is higher than a pre-computed high limit.

However, for this study, we have implemented what we believe is a better policy, which we call the dynamic energy level policy, explained below.

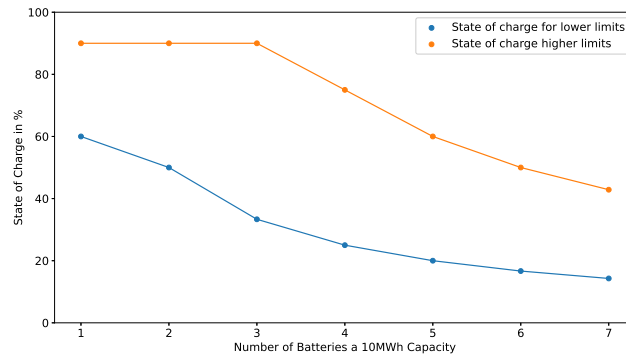


Figure 13. Low and high state-of-charge limits.

#### 4.1.1. Dynamic Energy Level Policy

Forecasts of the wind power can be used to estimate the remaining time before the battery system is depleted and unable to provide power. We define a forecast horizon  $\Delta T$ , with  $\Delta T$  slightly longer than the startup time of the gas turbines. We also assume that  $\Delta T$  is longer than the time between decision intervals,  $\Delta t$ , and for simplicity, we assume that  $\Delta T$  is a multiple of the decision interval  $\Delta T = n \cdot \Delta t$ .

If the current rate of change,  $D$ , of the state of charge remains constant, the state of charge  $SoC$  after time  $\Delta T$  can be estimated as:

$$SoC(t_0 + \Delta T) \approx SoC(t_0) + D\Delta T, \tag{11}$$

where  $t_0$  is the current time.

We assume a perfect wind forecast so that the available wind power  $AWP$  is known in the forecast horizon. The perfect forecast assumption can be relaxed, but we assume a perfect forecast here to simplify the derivation.

Then, the available wind energy,  $AWE$ , within the time interval  $[t_0, t_0 + \Delta T]$  is given by

$$AWE(t_0) = \sum_{i=0}^n AWP(t_0 + i\Delta t)\Delta t \tag{12}$$

The change in energy  $\Delta E_w$  generated from wind energy within the time interval  $[t_0, t_0 + \Delta T]$  relative to the persistent assumption is

$$\Delta E_w(t_0) = AWE(t_0) - AWP(t_0)\Delta T \tag{13}$$

We assume that the demand level stays constant since we have no method for predicting the change in demand.

Taking the prediction of available wind energy into account, the state of charge limits for starting the gas turbines can be relaxed.

The relaxed low level limit becomes:

$$SoC(t_0) + D\Delta t + \frac{\Delta E_w(t_0)}{E_{max}} \leq 0 \tag{14}$$

This means that the gas turbines are started if the battery system is estimated to be depleted after the time horizon  $\Delta T$ .  $\Delta E_w$  may be positive or negative.  $E_{max}$  is the energy capacity of the battery system.

#### 4.2. Policy for When to Stop the Gas Turbine System

Here, the question is when to give the signal to stop the gas turbine system and rely on the wind turbines and battery system to provide energy.

We proposed two policies for when to stop the gas turbine system.

##### 4.2.1. Fixed Level Policy

The policy in this case is simply to give the signal to switch off the gas turbines when the battery state of charge exceeds a preset level, as illustrated in Figure 13.

##### 4.2.2. Available Wind Power Policy

The policy in this case is to switch off the gas turbines if the available wind power alone is sufficient to meet the system's demands.

#### 4.3. Battery Policy

Degradation of the batteries due to usage can be an issue. We proposed and tested two policies for how to run the battery system.

##### 4.3.1. Maximal Power Output Policy

The policy is to utilize the whole capacity when charging and discharging the batteries. The battery system will, in this case, accept charging and discharging rates up to the maximal possible limits given in Equation (6).

##### 4.3.2. Limited Power Output Policy

The battery system will, under this policy, only utilize some defined fraction of the maximal charging and discharging rates, except in emergency situations where the needed power cannot be provided otherwise.

#### 4.4. Strategies

We define a control strategy using the different policies explained above and summarize them in Table 1.

**Table 1.** Simulated control strategies and their associated policies.

	Policy		
	Gas Turbines On	Gas Turbines Off	Battery Degradation
<b>Strategy 1</b>	Dynamic-level Section 4.1.1	Fixed-level Section 4.2.1	Limited power output at 10% Section 4.3.2
<b>Strategy 2</b>	Dynamic-level Section 4.1.1	Fixed-level Section 4.2.1	Maximum power output Section 4.3.1
<b>Strategy 3</b>	Dynamic-level Section 4.1.1	Available-wind-power Section 4.2.2	Limited power output at 10% Section 4.3.2
<b>Strategy 4</b>	Dynamic-level Section 4.1.1	Available-wind-power Section 4.2.2	Maximum power output Section 4.3.1

## 5. Simulations

In this section, we present the different simulation cases and their results. We will first present the different inputs and outputs in Section 5.1. In Sections 5.2 and 5.3, we present the input samples and their variations. In Section 5.4, we present the simulation results of an individual case to gain an intuition of the system dynamics, and later on in Section 5.5, we present the results of simulating the whole sample set in an aggregated manner.

### 5.1. Inputs and Outputs

The simulation cases were run by selecting time series of wind speed and power demand among 50 different samples of 7 days duration. These samples were then used to simulate different system scenarios by varying the number of wind turbines and batteries,

as well as the control strategies. The main simulation parameters are summarized in Table 2. The simulation results are summarized in Table 3.

**Table 2.** Overview of the simulation parameters.

Input	Description
Wind speed samples	We used 50 samples of 7 days, sampled at 1 h intervals and with interpolation possibilities to 1 s intervals
Power demand samples	We used 50 samples of 7 days, sampled at 1 h intervals and with interpolation possibilities to 1 s intervals
Batteries	We used battery units of a capacity of 10 MWh, with $C_{rate} = 0.5 \text{ h}^{-1}$ and $D_{rate} = 1 \text{ h}^{-1}$ . We varied the number of batteries between 1 and 7, which correspond to variation of energy storage capacity between 10 MWh and 70 MWh. Varying the number of batteries was modelled as one large battery and parameterized using $E_{max} \in \{10, 20, 30, 40, 50, 60, 70\}$ MWh
Wind turbines	We used wind turbine units of a capacity of 10 MWh and varied their number between 1 and 7, corresponding to variation of maximum wind power generation between 10 MWh and 70 MWh
Gas turbines	We used 3 gas turbine units of a maximum power of 12 MW each
Control strategy	We simulated the four control strategies that are defined in Table 1

**Table 3.** Overview of the recorded simulation results.

Output	Description
Wind turbines	A time series of available wind power $AWP$ and generated wind power $P_{wind}$ from Equation (5) presented in MW
Gas turbines	A time series of the emission rates $E_{co2}$ and $E_{nox}$ presented in $\text{kg s}^{-1}$ , and the generated power $P_{gt}$ from Equation (3)
Battery	A time series of the battery state of charge $SoC$ presented in % and the power delivered or consumed $P_{bat}$ presented in MW
Simulation metrics	A time series of the system stability $S_{st}$ and quality $S_{qt}$ from Equation (7)
Stochastic metrics	Total $\text{CO}_2$ emissions relative to a base case with gas turbines only and battery degradation from Equation (10)

### 5.2. Wind Speed Inputs

The wind speed samples were generated by picking a start time at random from the downloaded time series in Section 2.7. Figure 14 shows some of the characteristics of the wind speed samples used in the simulations. The figures show relatively important variations with cases where the wind speed is frequently high, such as in case numbers 20 and 40, and relatively low, such as in case numbers 48 and 49.

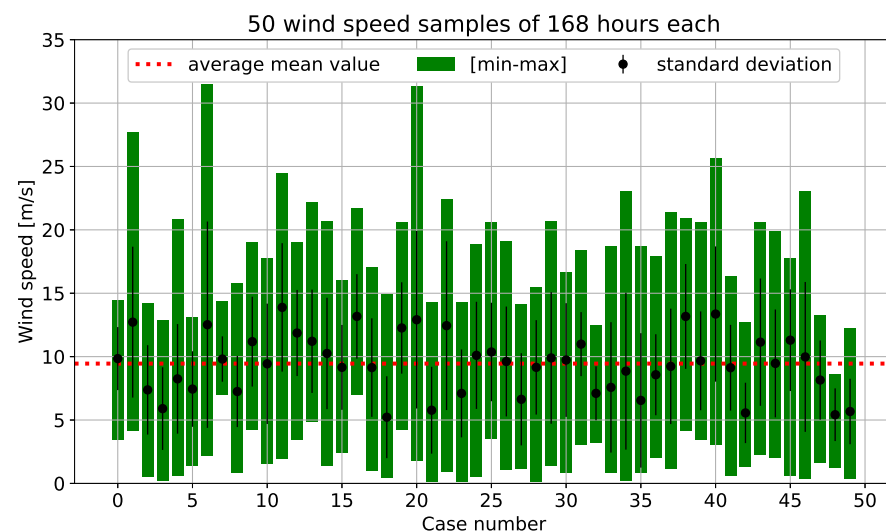


**Figure 14.** Wind speed variation for 50 samples containing 7 day records at 100 s intervals.

### 5.3. Power Demand Inputs

The power demand samples were generated with the GHMM model in Section 2.6. The variation of the power demand can also be observed in Figure 15. A typical example of high demand in this study would be case number 43, while case number 7 can be considered a low-demand scenario.

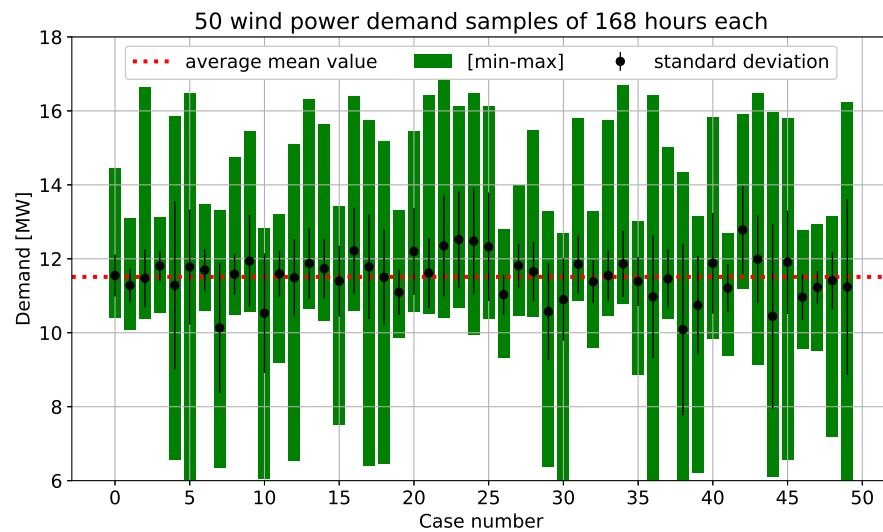


**Figure 15.** Power demand variation for 50 samples containing 7-day records at 100 s intervals.

#### 5.4. Simulation Case Example

For illustration, we present a case with a relatively low wind speed and contrast it with a case with relatively high wind speed. To illustrate some differences of the strategy choices, we ran the simulations for Strategy 1 and Strategy 4 from Table 1. The first thing to notice is that the system is energy-stable for all four simulations, as the *Stability* variable  $S_{st}$  equals 1 for all cases. However, we notice that the system quality is higher for the cases with high wind speed (Figures 16 and 17) than in those with low wind speed (Figures 18 and 19), which is, as expected, proportional to the rate of CO<sub>2</sub> emissions. However, we can notice important differences between the two strategies in the periods where the gas turbines are engaged, as well as in the state of charge of the batteries. Analysis of single simulation cases give insight into how the energy management strategies work in specific scenarios. However, to provide answers about which strategy is best, we have to look at ensembles of simulation results.

#### 5.5. Simulation with Stochastic Inputs

Deriving conclusions from individual simulations has been shown to be challenging. For this reason, we aimed to simplify the analysis by aggregating the relevant simulation results and excluding observations that had less relevance. These are stability and quality results. The stability was stable at a value of 1 ( $S_{st} = 1$ ) for all the simulation cases that we ran, making it less relevant for our case study. However, for scenarios where the demand becomes higher than the capacity of the system, the stability can be a useful concept to exploit. The quality, as we have defined it in this paper, depends on the stability of the system and the CO<sub>2</sub> emission rate, but since the stability was constantly equal to 1, we considered it irrelevant for the remaining analysis.

To analyse the simulations, we focused on two observations. The first one was the amount of CO<sub>2</sub> emissions relative to the case where the whole power demand was supplied using gas turbines (today's situation), which we refer to as the *baseline* case. This is presented in Section 5.5.1. The second one is the battery life time.

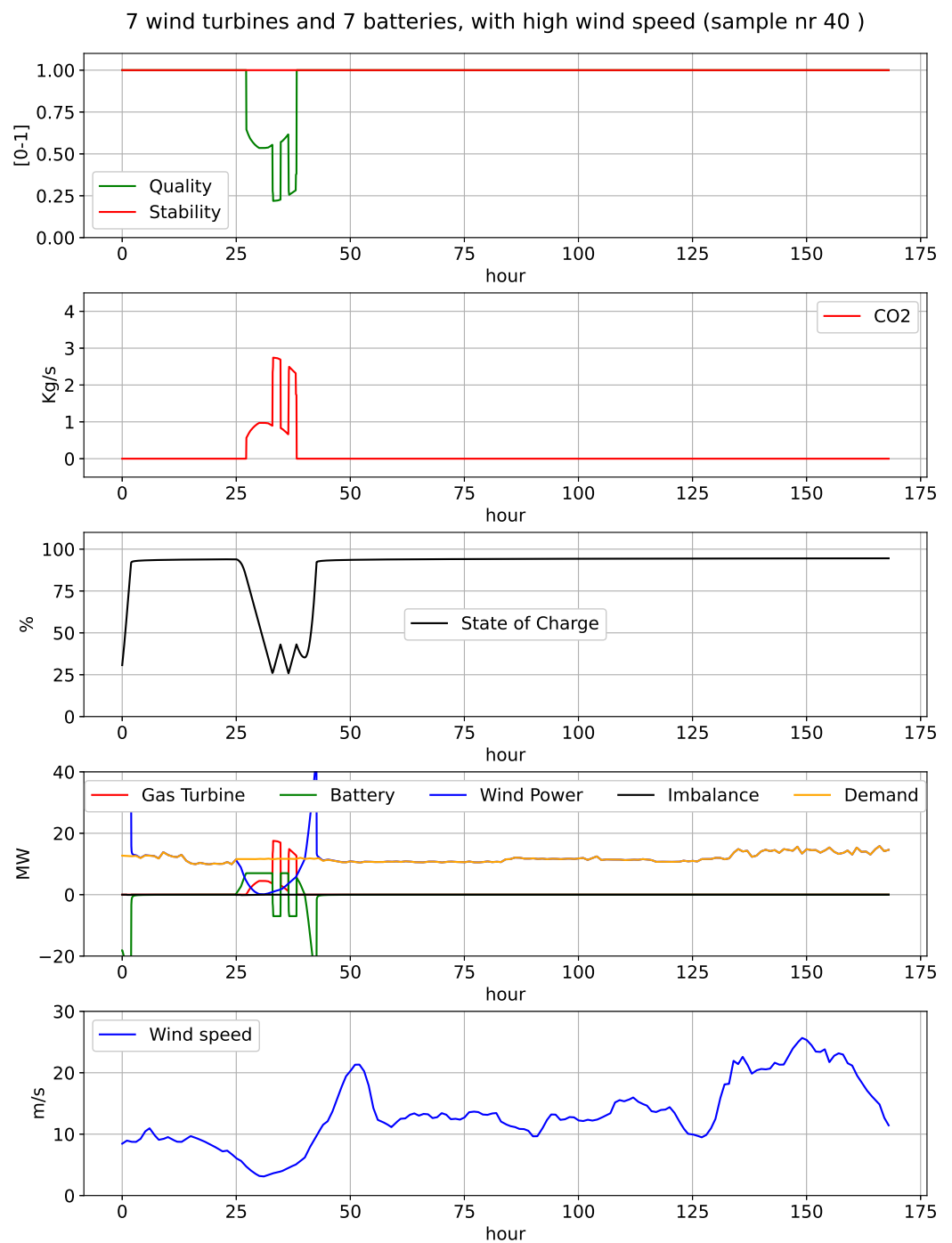


Figure 16. Strategy 1 with high wind speed scenario.

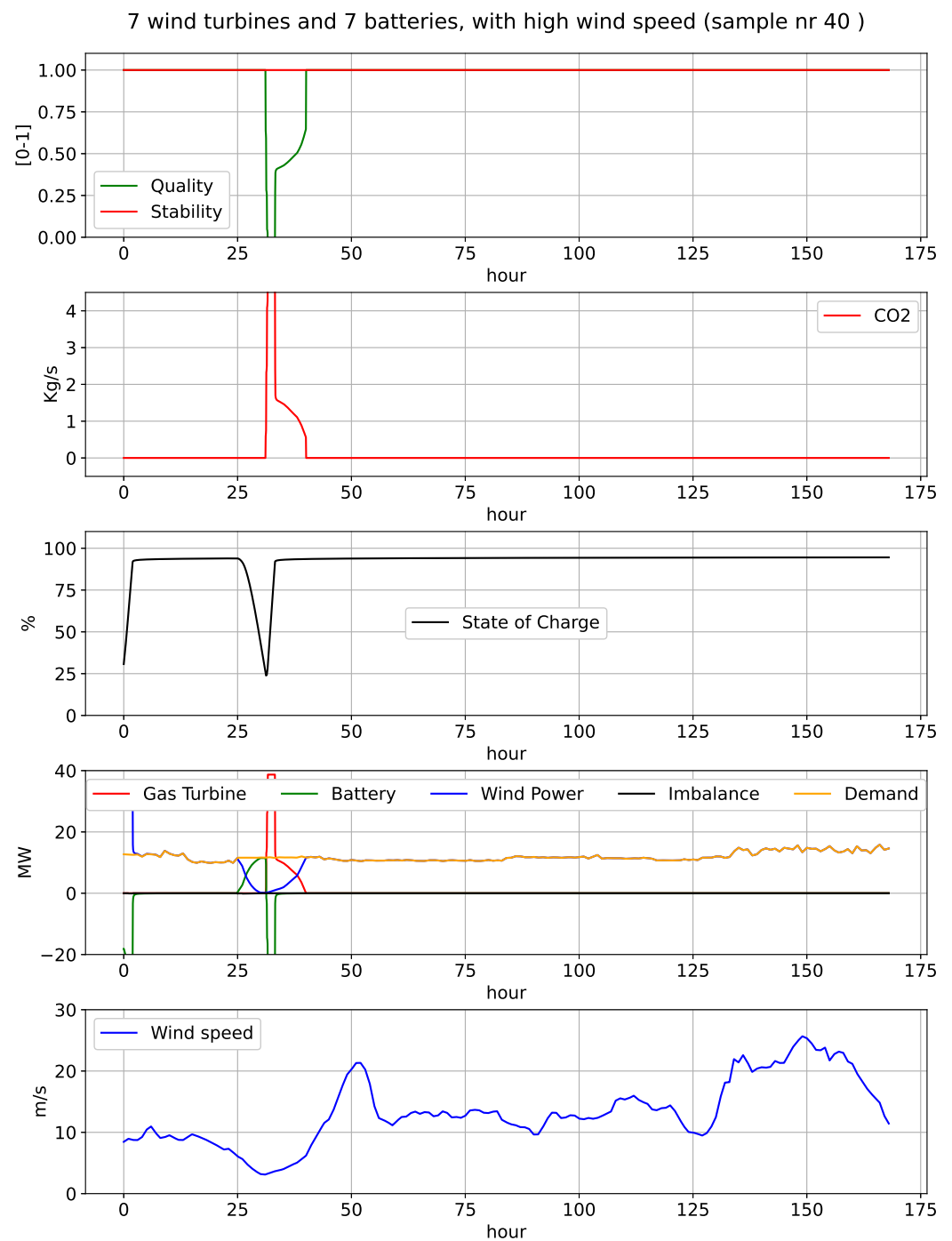


Figure 17. Strategy 4 with high wind speed scenario.

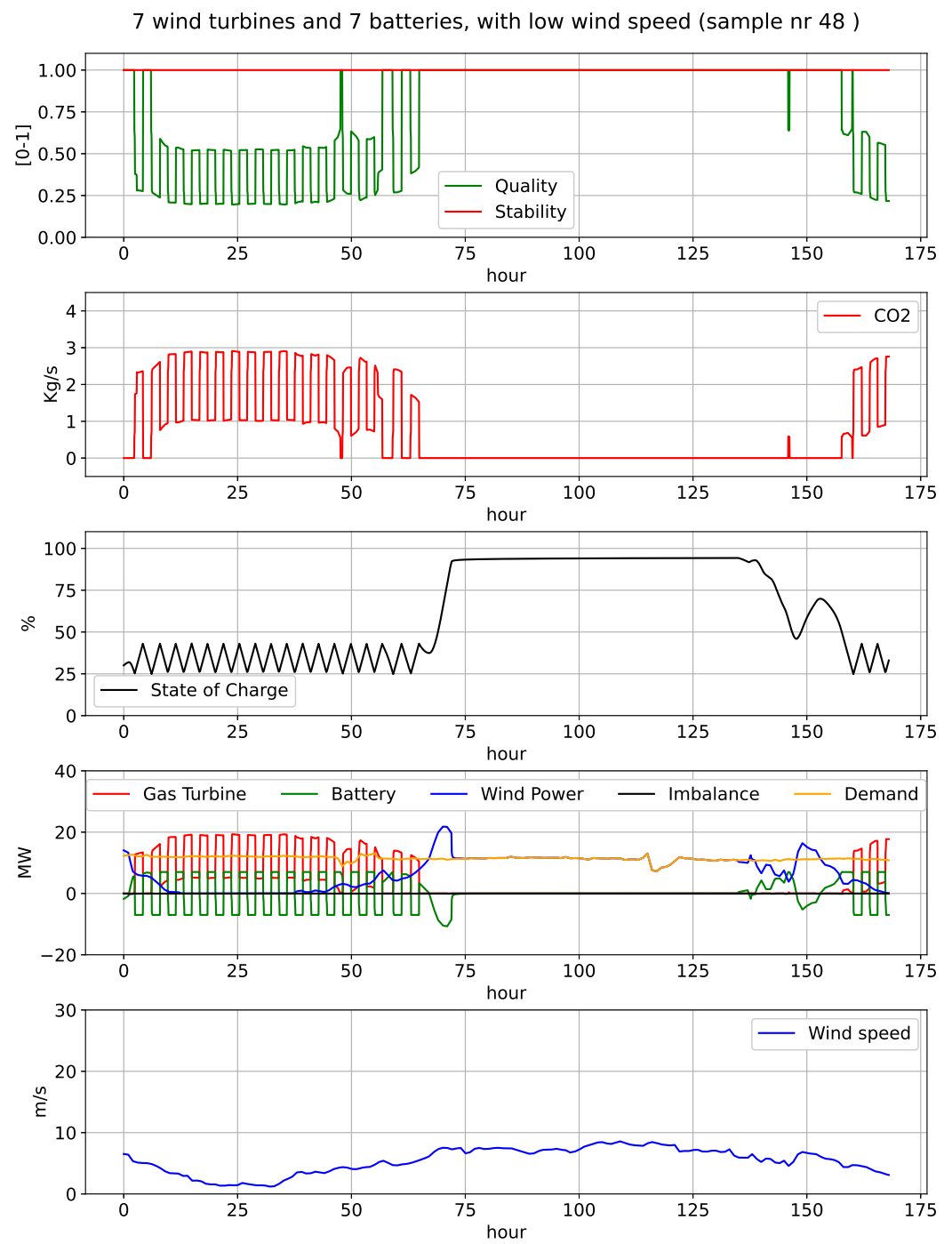
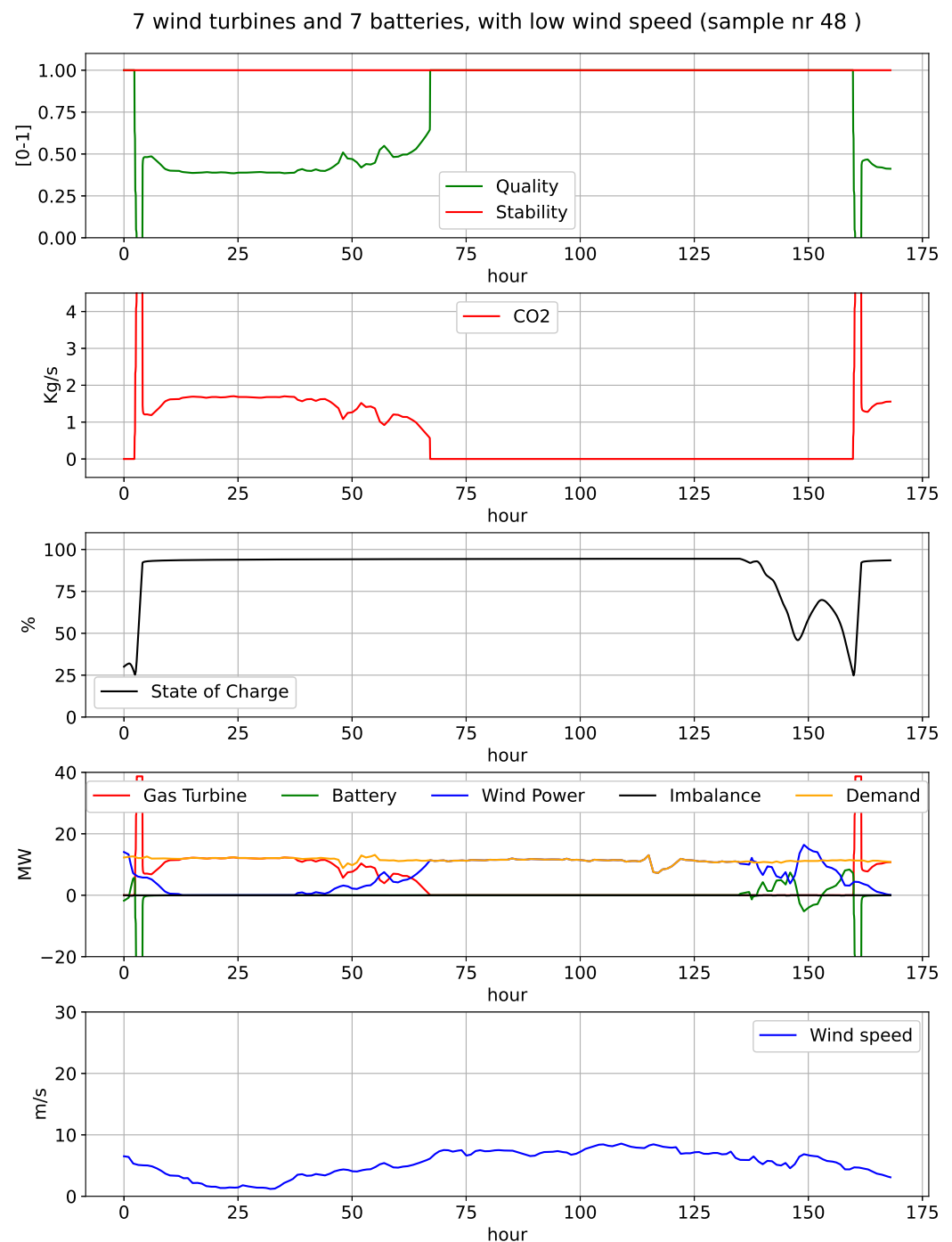


Figure 18. Strategy 1 with low wind speed scenario.



**Figure 19.** Strategy 4 with low wind speed scenario.

### 5.5.1. CO<sub>2</sub> Emissions Results

For every simulation case, the CO<sub>2</sub> emissions were integrated for the whole simulation period to obtain the total amount of emissions. These total amounts were normalized with the *baseline* emissions (no wind turbines or batteries) and then averaged for the whole set of samples (wind speed and power demand). The results are shown in Figures 20–23. In the figures, the values in the cells stand for the % emissions relative to *baseline* when we allow the gas turbines to be switched off completely (0 emissions), as well as the % emissions when a single gas turbine is kept idle (shown in parentheses) with a minimum CO<sub>2</sub> emission rate of 0.5 kg s<sup>-1</sup> (today's practice). As a first observation, we notice the significant increase in CO<sub>2</sub> emissions when keeping a gas turbine idle, and this is regardless

of the strategy, the number of batteries, and the number of wind turbines. We notice that the applied strategies have a comparable effect with respect to CO<sub>2</sub> emissions, where Strategy 2 performs slightly better. We also notice that the impact of adding wind turbines appears to be significantly more important than the impact of adding batteries, although this effect is less significant for Strategy 2.

The results show that the CO<sub>2</sub> emissions can be reduced by up to around 80% depending on the configuration and up to 55% if one gas turbine is kept idle.

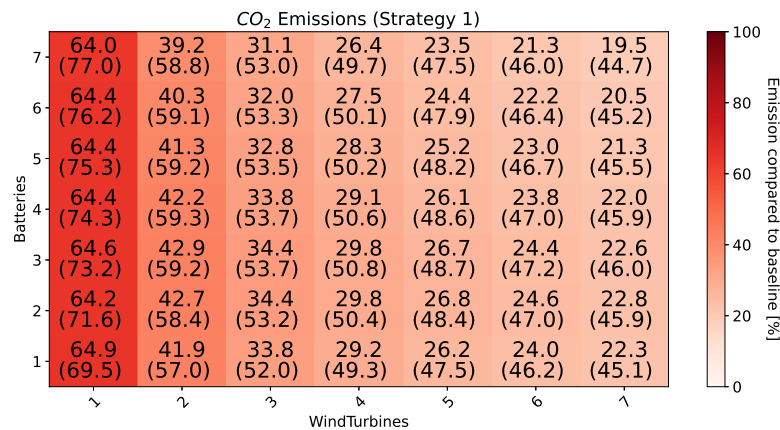


**Figure 20.** CO<sub>2</sub> emissions relative to baseline when the gas turbines can be turned off completely (0 emissions) or are kept idle with an emission rate of 0.5 kg s<sup>-1</sup>, shown in parentheses.

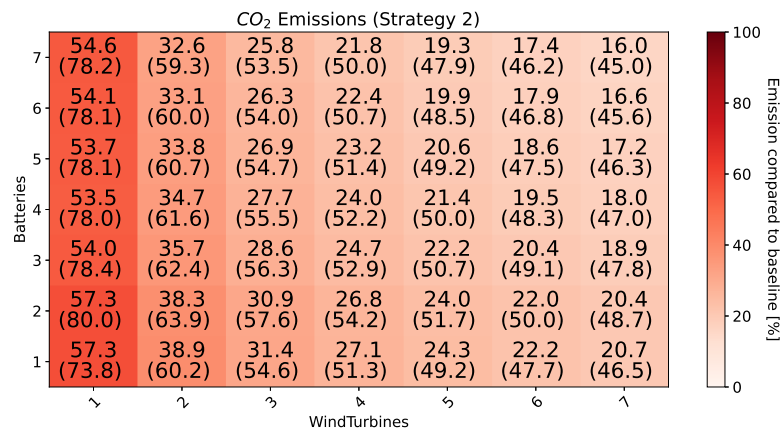


**Figure 21.** CO<sub>2</sub> emissions relative to baseline when the gas turbines can be turned off completely (0 emissions) or are kept idle with an emission rate of 0.5 kg s<sup>-1</sup>, shown in parentheses.

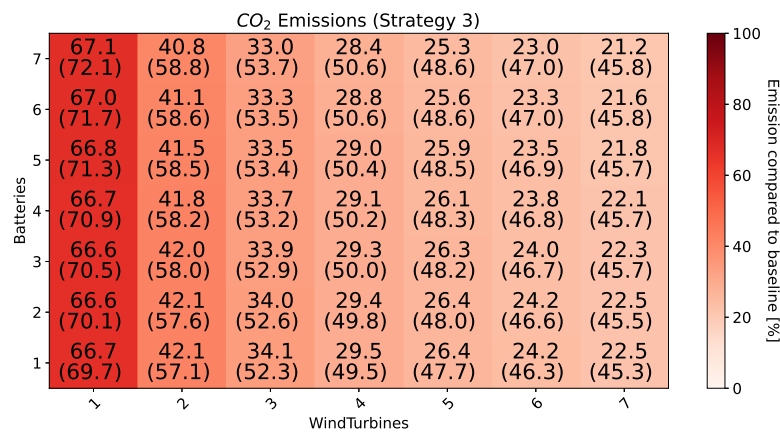


**Figure 22.** CO<sub>2</sub> emissions relative to baseline when the gas turbines can be turned off completely (0 emissions) or are kept idle with an emission rate of 0.5 kg s<sup>-1</sup>, shown in parentheses.

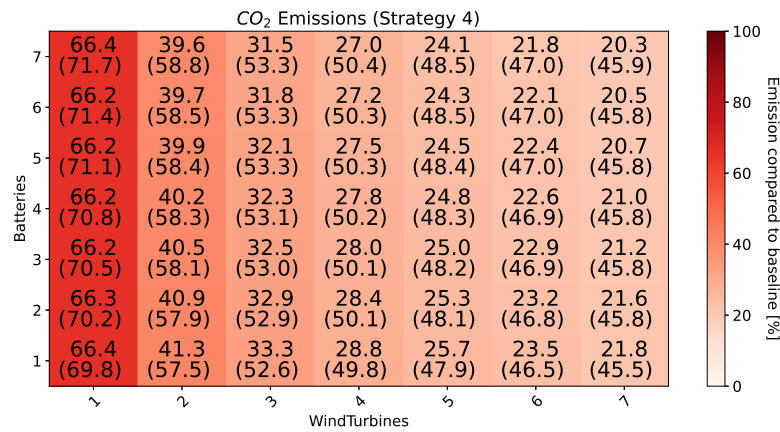


**Figure 23.** CO<sub>2</sub> emissions relative to baseline when the gas turbines can be turned off completely (0 emissions) or are kept idle with an emission rate of 0.5 kg s<sup>-1</sup>, shown in parentheses.

### 5.5.2. Battery Degradation

The aggregated battery degradation for the strategies in Table 1 are presented in Figures 24–27 using the rainflow counting algorithm from Section 3.

Using the fifty one-week simulations for each combination of wind turbines and batteries, we computed the average degradation per week and extrapolated the result to the equivalent degradation over 20 years. A degradation of more than 100% means that the batteries will have reached their end of life before the first 20 years of operation.

It may be surprising that the degradation that occurs with only one wind turbine using strategy 3 and 4 is clearly less than when having more wind turbines. The reason for this is that one wind turbine is usually not sufficient to supply the demand. Therefore, the gas turbines will have to run most of the time in this case, leading to less demand on the batteries.

There is also more degradation when using two batteries compared to one battery, which can be seen clearly for strategies 1 and 2. The reason for this is that one battery is often not sufficient to provide the needed power, and therefore, the gas turbines will have to run most of the time in this case. However, if there are two or more batteries, the gas turbines can be switched off more often, leading to more degradation of the batteries.

The results show that the battery system can be expected to last more than 20 years for strategies 3 and 4 and more than 20 years for strategy 1 if the number of wind turbines is greater than 3. However, strategy 2 leads to severe strain on the batteries due to the power cycling.

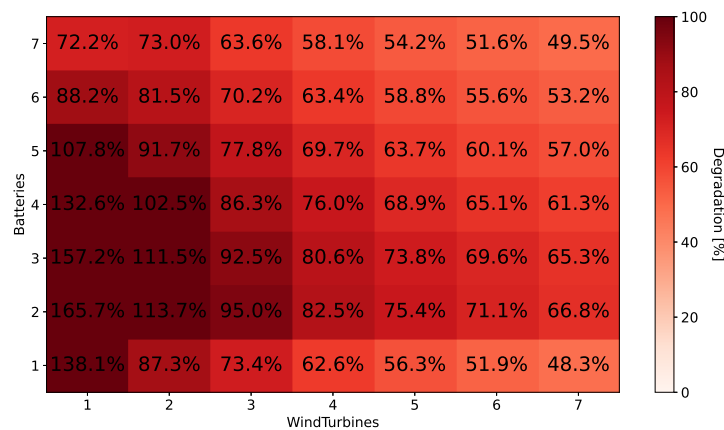


**Figure 24.** Degradation of the batteries over 20 years of usage with strategy 1.

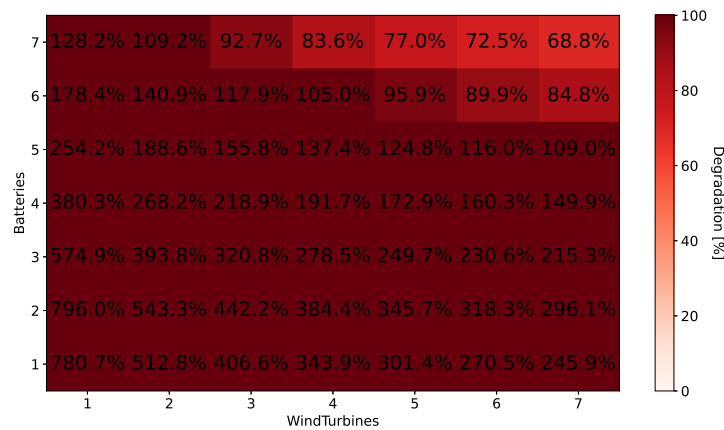


Figure 25. Degradation of the batteries over 20 years of usage with strategy 2.

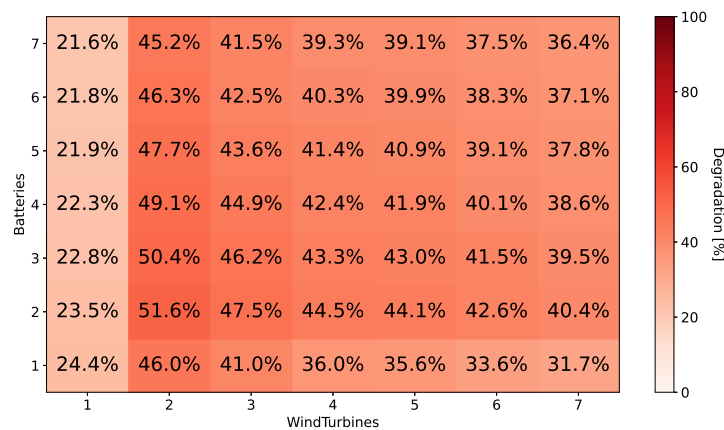


Figure 26. Degradation of the batteries over 20 years of usage with strategy 3.



Figure 27. Degradation of the batteries over 20 years of usage with strategy 4.

### 6. Conclusions

In this paper, we have provided details about a flexible power simulation model and used it to evaluate control strategies and design options for a system of offshore wind turbines and battery systems to provide power to offshore installations without a grid connection to the land. All the proposed control strategies provide a stable energy supply but differ in the estimated CO<sub>2</sub> emissions and the estimated battery degradation. If one gas turbine is kept idle all the time, the CO<sub>2</sub> emissions can be reduced by 30–55%, depending on the control strategy, the number of wind turbines, and the number of batteries. However, if all the gas turbines are shut completely down when they are not needed, the CO<sub>2</sub> emissions may be reduced by more than 80% given sufficient wind power capacity. The simulations show that with sufficient battery capacity, it is possible to shut down the gas

turbines for extended periods of time and start them on demand, thus enabling significant reductions in CO<sub>2</sub> emissions compared to running the gas turbines in idle mode. The battery storage can be controlled in a way that does not severely limit its lifetime, and it is estimated not to have spent more than approximately 50% of its lifetime within the first 20 years for strategies 3 and 4 when using two or more wind turbines.

The component models are quite simple and are parameterized, which enable calibration and validation with measurements in realistic situations to give good approximations to reality, as we have done for the batteries. For the validation of the other components of the model, we propose to use measurements in the lab or the field. The demand side can be more flexible than we have assumed in this study. It may be possible to delay energy-demanding processes on oil and gas installations until sufficient wind power is available. Such flexibility may be exploited to enable further reductions in CO<sub>2</sub> emissions.

For further work, we propose to optimize both the control and design options to maximize the system quality as introduced in Section 2.8 and redefine it by including other costs, such as delaying energy demanding processes, the carbon tax, the investment and operational costs of the battery systems, and the investment and operational costs of wind farms. The cost of the resulting system should be compared to estimates of the cost of the alternative, which is electrification of the oil and gas installations using land cables and connection to the onshore grid.

**Author Contributions:** Conceptualization, N.S. and Y.H.; methodology, N.S. and Y.H.; software, N.S. and Y.H.; validation, N.S. and Y.H.; formal analysis, N.S. and Y.H.; investigation, N.S. and Y.H.; resources, N.S. and Y.H.; data curation, N.S. and Y.H.; writing—original draft preparation, N.S. and Y.H.; visualization, N.S. and Y.H.; supervision, Y.H.; project administration, Y.H.; funding acquisition, Y.H. All authors have read and agreed to the published version of the manuscript.

**Funding:** This work was conducted as part of the project Electrification of Oil and Gas Installation by Offshore Wind (308838–KSPKOMPETANSE19) funded by The Research Council of Norway and with financial support of Equinor Energy AS, ConocoPhillips Skandinavia AS, and Aibel AS.

**Data Availability Statement:** Wind speed data is available from <https://cds.climate.copernicus.eu> (accessed on 21 February 2023). Battery calibration data is available at [12]. The data of the reference wind turbine is available at [11]. Restrictions apply to the availability of the gas turbine data. These data was obtained from Equinor and are available with the permission of Equinor.

**Conflicts of Interest:** The authors declare no conflict of interest.

## Abbreviations

The following abbreviations are used in this article:

$AWP$	Available wind power	$AWE$	Available wind energy
$\rho_{air}$	Air density	$A$	Wind turbine swept area
$BIC$	Bayesian Information Criterion	$N_{wt}$	Number of wind turbines
$C_{lim}$	Charging power limit	$C_{rate}$	Battery Charging rate
$C_p$	Performance power coefficient of wind turbine	$D_{lim}$	Discharging power limit
$D$	Total battery degradation	$E_{co2}$	CO <sub>2</sub> emissions
$E_{max}$	Energy capacity of battery	$E_{nox}$	NOx emissions
$GHMM$	Gaussian Hidden Markov Model	$N_{wt}$	Number of wind turbines
$P_{base}$	Base power	$P_{bat}$	Battery power
$P_d$	Demand power	$P_{gt}$	Gas turbine's power
$P_{imb}$	Power imbalance	$P_{wind}$	Wind farm power
$S_{qt}$	System quality	$S_{st}$	System stability
$SoC$	State-of-charge	$\eta_c$	Battery charging efficiency
$\eta_d$	Battery discharging efficiency	$c_0$	Sigmoid's midpoint on charge
$d_0$	Sigmoid's midpoint on discharge	$k_c$	Steepness of charge
$k_d$	Steepness of discharge	$\rho u$	Per unit

## References

1. Statistics Norway. *Emissions to Air*; 2022. Available online: <https://www.ssb.no/en/natur-og-miljo/forurensning-og-klima/statistikk/utslipp-til-luft> (accessed on 21 February 2023).
2. Teevan, C.; Medinilla, A.; Sergejeff, K. The Green Deal in EU foreign and development policy. ECDPM Briefing Note 2021. Available online: <https://ecdpm.org/work/the-green-deal-in-eu-foreign-and-development-policy> (accessed on 21 February 2023).
3. Al-Haiki, Z.E.; Shaikh-Nasser, A.N. Power transmission to distant offshore facilities. *IEEE Trans. Ind. Appl.* **2011**, *47*, 1180–1183. [[CrossRef](#)]
4. Solbrekke, I.M.; Sorteberg, A.; Haakenstad, H. The 3 km Norwegian reanalysis (NORA3)—A validation of offshore wind resources in the North Sea and the Norwegian Sea. *Wind. Energy Sci.* **2021**, *6*, 1501–1519. [[CrossRef](#)]
5. Saadallah, N.; Heggelund, Y. An Approach for Reducing Gas Turbines Usage by Wind Power and Energy Storage. In Proceedings of the 14th International Modelica Conference, Linköping, Sweden, 20–24 September 2021; pp. 627–632. [[CrossRef](#)]
6. Fellah, K.; Abbou, R.; Khiat, M.; Rahiel, D. Comparative study of battery energy storage systems in a micro-grid based on real-time simulation. *Indones. J. Electr. Eng. Informatics (IJEI)* **2021**, *9*, 371–383. [[CrossRef](#)]
7. MacRae, N.; Batteh, J.; Velut, S.; Skrivan, W.; Khan, I.; Jang, D. Micro-grid Design and Cost Optimization using Modelica. In Proceedings of the American Modelica Conference 2020, Boulder, CO, USA, 23–25 March 2020; pp. 18–27. [[CrossRef](#)]
8. Malekshah, S.; Alhelou, H.H.; Siano, P. An optimal probabilistic spinning reserve quantification scheme considering frequency dynamic response in smart power environment. *Int. Trans. Electr. Energy Syst.* **2021**, *31*, e13052. [[CrossRef](#)]
9. Nakabi, T.A.; Toivanen, P. Deep reinforcement learning for energy management in a microgrid with flexible demand. *Sustain. Energy Grids Networks* **2021**, *25*, 100413. [[CrossRef](#)]
10. Rogalev, A.; Rogalev, N.; Kindra, V.; Komarov, I.; Zlyvko, O. Research and Development of the Combined Cycle Power Plants Working on Supercritical Carbon Dioxide. *Inventions* **2022**, *7*, 76. [[CrossRef](#)]
11. Bak, C.; Zahle, F.; Bitsche, R.; Kim, T.; Yde, A.; Henriksen, L.C.; Hansen, M.H.; Blasques, J.P.A.A.; Gaunaa, M.; Natarajan, A. The DTU 10-MW Reference Wind Turbine. In Proceedings of the Danish Wind Power Research 2013, 27–28 May 2013. Trinity, Fredericia, Denmark.
12. Sandia National Laboratories Grid Energy Storage Department; Battery Archive: 2021. Available online: <https://www.batteryarchive.org> (accessed on 21 February 2023).
13. Baum, L.E.; Petrie, T. Statistical inference for probabilistic functions of finite state Markov chains. *Ann. Math. Stat.* **1966**, *37*, 1554–1563. [[CrossRef](#)]
14. Dias, J.G.; Vermunt, J.K.; Ramos, S. Clustering financial time series: New insights from an extended hidden Markov model. *Eur. J. Oper. Res.* **2015**, *243*, 852–864. [[CrossRef](#)]
15. Liu, Y.; Ye, L.; Qin, H.; Hong, X.; Ye, J.; Yin, X. Monthly streamflow forecasting based on hidden Markov model and Gaussian Mixture Regression. *J. Hydrol.* **2018**, *561*, 146–159. [[CrossRef](#)]
16. Hermias, J.P.; Teknomo, K.; Monje, J.C.N. Short-term stochastic load forecasting using autoregressive integrated moving average models and Hidden Markov Model. In Proceedings of the 2017 International Conference on Information and Communication Technologies (ICICT), IEEE, Karachi, Pakistan, 30–31 December 2017; pp. 131–137.
17. Schwarz, G. Estimating the dimension of a model. *Ann. Stat.* **1978**, 461–464. [[CrossRef](#)]
18. Matsuishi, M.; Endo, T. Fatigue of metals subjected to varying stress. *Jpn. Soc. Mech. Eng. Fukuoka Jpn.* **1968**, *68*, 37–40.
19. Chawla, M.; Naik, R.; Burra, R.; Wiegman, H. Utility energy storage life degradation estimation method. In Proceedings of the 2010 IEEE Conference on Innovative Technologies for an Efficient and Reliable Electricity Supply, IEEE, Waltham, MA, USA, 27–29 September 2010; pp. 302–308.
20. Alam, M.; Saha, T. Cycle-life degradation assessment of Battery Energy Storage Systems caused by solar PV variability. In Proceedings of the 2016 IEEE Power and Energy Society General Meeting (PESGM), Boston, MA, USA, 17–21 July 2016; pp. 1–5.

**Disclaimer/Publisher’s Note:** The statements, opinions and data contained in all publications are solely those of the individual author(s) and contributor(s) and not of MDPI and/or the editor(s). MDPI and/or the editor(s) disclaim responsibility for any injury to people or property resulting from any ideas, methods, instructions or products referred to in the content.